White Rose Research Online

eprints@whiterose.ac.uk
https://eprints.whiterose.ac.uk
Universities of Leeds, Sheffield and York

Deposited via The University of Sheffield.

White Rose Research Online URL for this paper:
https://eprints.whiterose.ac.uk/id/eprint/190539/

Version: Published Version

Article:
Osman, T., Lim, L.W., Ng, J.S. et al. (2022) Fabrication of infrared linear arrays of InAs planar avalanche photodiodes. Optics Express, 30 (12). p. 21758.

https://doi.org/10.1364/oe.460017

Reuse
This article is distributed under the terms of the Creative Commons Attribution (CC BY) licence. This licence allows you to distribute, remix, tweak, and build upon the work, even commercially, as long as you credit the authors for the original work. More information and the full terms of the licence here: https://creativecommons.org/licenses/

Takedown
If you consider content in White Rose Research Online to be in breach of UK law, please notify us by emailing eprints@whiterose.ac.uk including the URL of the record and the reason for the withdrawal request.

Research Article | Vol. 30, No. 12 / 6 Jun 2022 / Optics Express 21758

Optics EXPRESS

Check for updates

Fabrication of infrared linear arrays of InAs planar avalanche photodiodes

T. Osman, L. W. Lim, J. S. Ng, and C. H. Tan*

Department of Electrical and Electronic Engineering, The University of Sheffield, Mappin Street, Sheffield S1 3JD, UK

*c.h.tan@sheffield.ac.uk

Abstract: We report a, to the best of our knowledge, new device fabrication process for 128-pixel linear arrays of InAs planar avalanche photodiodes, utilizing selective area implantation of Beryllium ions into epitaxially-grown InAs wafers. The pixels exhibited uniform avalanche gain and responsivity. Room temperature responsivity values at 1550 and 2004 nm wavelengths are 0.49 ± 0.017 and 0.89 ± 0.024 A/W, respectively. Reverse dark current-voltage and avalanche gain measurements were carried out at different temperatures (from room temperature to 150 K). At 200 K at −15 V reverse bias, the pixels exhibited an avalanche gain of 22.5 ± 1.18 and dark current density of 0.68 ± 0.48 A/cm^2.

Published by Optica Publishing Group under the terms of the Creative Commons Attribution 4.0 License. Further distribution of this work must maintain attribution to the author(s) and the published article's title, journal citation, and DOI.

1. Introduction

Indium Arsenide (InAs) is one of the semiconductor materials used in infrared (IR) avalanche photodiodes (APDs). It has a direct bandgap of 0.34 eV, corresponding to 3.55 µm cut-off wavelength at room temperature, so InAs APDs provide high detection efficiency in the short-wave infrared (SWIR) wavelengths. Its spectral response makes it an ideal detector choice for remote sensing of common atmospheric gasses such as methane at 1.67 µm [1,2] and 3.4 µm [3] and carbon dioxide at 2 µm [4].

Currently, HgCdTe is one of the most popular materials for fabricating IR detectors. By controlling the Hg composition, HgCdTe can be used to respond to a large span of wavelengths from 0.7 µm to 25 µm [5]. There have been many successful demonstrations of HgCdTe single pixel, focal plane array and linear array photodiodes and APDs [6,7]. HgCdTe based detectors are, however, difficult to grow, requiring costly CdTe substrates to minimise crystal defects. Most of them also require cryogenic operation temperature ~ 80K. Additionally, environmental concerns have led to efforts to phase out the use of Hg in new products [8]. Hence, HgCdTe photodiodes are mainly utilized in specialised and military applications. InSb APDs also exhibit a photo-response into the mid-wave IR. With a bandgap of 0.17 eV at room temperature, it can detect wavelengths up to 7.3 µm. At 80 K the bandgap expands to 0.23 eV, reducing the cut-off wavelength to 5.4 µm [9]. However, like HgCdTe, InSb photodetectors too require cryogenic cooling to suppress leakage currents. Another material capable of detecting into the SWIR is $In_{0.8}Ga_{0.2}As$, hereafter referred to as extended InGaAs, which exhibits a room temperature cut-off wavelength of 2.6 µm. Since extended InGaAs is no longer lattice-matched to InP substrates, wafer growth requires the use of InGaAs or InAsP buffer layers on InP substrates, resulting in growth defects. This issue is exacerbated when the gallium content is further reduced to achieve longer cut-off wavelengths. Despite these limitations large format extended InGaAs arrays have been reported operating at 200 K [10]. Type-II superlattice (T2SL) structures such as the $In_{0.53}Ga_{0.47}As/GaAs_{0.5}Sb_{0.5}$ structure found in [11] can also be engineered to respond to SWIR wavelengths. However, they are unable to provide avalanche gain on their own and

#460017
Journal © 2022

https://doi.org/10.1364/OE.460017
Received 6 Apr 2022; revised 19 May 2022; accepted 20 May 2022; published 1 Jun 2022

more complicated separate-absorption-multiplication (SAM) structures are required to enhance sensitivity.

Both InAs and certain compositions of HgCdTe are well established as classes of APDs known as electron avalanche photodiodes (eAPDs). This class of APDs is favoured as the ionisation coefficient ratio ($k = \beta/\alpha$, where β and α are the ionisation coefficients for holes and electrons respectively) is zero. This results in highly deterministic gain which produces very low excess noise and very high gain bandwidth products [12,13]. InSb is also predicted to show eAPD characteristics based on Monte Carlo simulations and excess noise measurements [14,15].

The vast majority of reported InAs APDs have used a mesa topology. This topology is not ideal for commercial fabrication, since the level of surface leakage currents depend critically on the device surface conditions [16]. A further limitation of mesa topology is the anisotropic nature of the wet etch used. This places a minimum size limit on the mesa diodes. Consequently, the high device yield and fill factor required for functional arrays of InAs photodetectors remains a challenge. To overcome this, recent studies have focused on planar InAs photodetectors [17,18], demonstrating selective area ion implantation in InAs. McNally demonstrated 4×4 arrays of planar InAs detectors using S^+ ion implantation into p-type InAs substrates [19]. However, there was little information regarding the uniformity of the arrays. Sandall *et al.* demonstrated mesa topology InAs APD arrays with highly uniform gain and dark current characteristics [20]. To the best of our knowledge there has been no report of development of large format planar InAs avalanche photodiodes.

In this paper, we report the first planar linear array of InAs APDs, fabricated using ion implantation. We observed good pixel uniformity in terms of gain, responsivity, and external quantum efficiency at 1520 and 2004 nm. Reverse and forward currents have been assessed at a range of temperatures from 300 to 150 K.

2. Experimental details

The wafer used in this work was grown by metalorganic vapor chemical vapor deposition (MOCVD) on a 2-inch n-type InAs substrate. The wafer structure consisted of 1 µm of Si doped n-InAs layer, followed by 6 µm of i-InAs. A 13×3 mm sample was cleaved from the wafer to accommodate 4 rows of the linear array. The sample was patterned with a SiO_2 encapsulating layer ~ 35 nm thick. It was then masked with photoresist and the p-type region was defined by Be ion implantation. Implantation was carried out with the sample at room temperature with 34 keV implant energy, 2×10^{14} cm^2 dosage, and 7 ° tilt angle (to minimize channeling effects).

After removing the photoresist, the sample underwent post-implant annealing for 15 minutes at 500°C. This was followed by removal of the SiO_2 encapsulating layer with a 10% HF solution. The p- and n- metal contacts were formed using thermal evaporation of Ti/Au onto the top of the device and the substrate, respectively. A thin SiN layer was deposited via plasma enhanced chemical vapor deposition (PECVD). The bond pad landing sites were then defined using standard photolithography techniques and the remaining SiN was etched using reactive ion etching (RIE). The SiN pattern provides isolation between the bond-pads and semiconductor surface as well as acting as a basic anti-reflection coating within the optical windows. The thickness of the SiN was not optimized as an antireflection (AR) coating. The bond-pads were then deposited onto the SiN, by thermal evaporation of Ti/Au. Finally, the remaining exposed surfaces were passivated with SU-8 to preserve the surface condition directly after the sample was subjected to a clean in 40% HF to remove any native oxides.

At the end of the device fabrication, the sample consists of four linear arrays of InAs planar photodiodes. Each array has 128 devices, with a dimension of 80×80 µm. A photograph of the section of the linear array is shown in Fig. 1(left). A common cathode is shared by all the devices via a back contact. The spacing between adjacent pixels was 15 µm, which is sufficient

for pixel isolation [17]. Figure 1(right) illustrates schematically the cross-section view of two neighboring photodiodes.

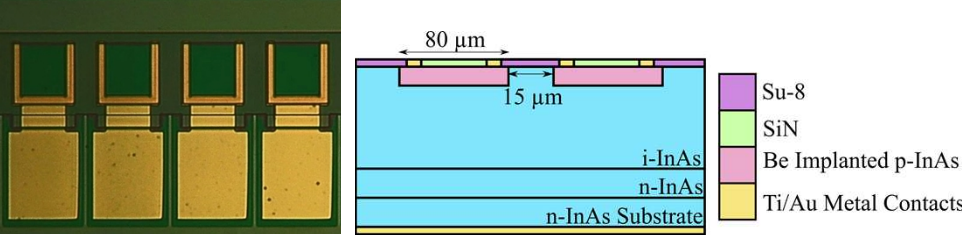

Fig. 1. Photograph of the fabricated linear array of APDs (left) and cross-sectional schematic depicting two adjacent InAs APDs (right).

Device characterization was carried out using a Janis ST-500 low-temperature probe station and a Keithley 236 source-measurement-unit. Responsivity measurements were performed at 1550 and 2004 nm wavelengths, using continuous-wave He-Ne and diode lasers respectively. Illumination from the lasers was delivered to the device-under-test by positioning the end of a single-mode fiber on top of the device's optical window. For avalanche gain measurements, phase sensitive detection (PSD) was employed utilizing an SR-830 lock-in amplifier and internal modulation of the 1550 nm wavelength diode laser.

3. Results and discussion

The mean dark current density across 87 devices from a single array at different temperatures is shown in Fig. 2 (left). At a reverse bias of −0.5 V the mean dark current drops by ~3 orders of magnitude, from 1.7 A/cm^2 at 300 K to 1.8 mA/cm^2 at 150 K. The low reverse bias dark current density at 200 K is ~ 60 times larger than that reported for extended InGaAs [10]. However, extended InGaAs exhibits a shorter cut-off wavelength (and hence a larger bandgap) than InAs. At room temperature, the dark current density is slightly higher than the planar InAs APDs found in [17,18]. Fitting the forward currents in Fig. 2. (left) yielded diode ideality factor values between 1.68–1.77. This suggests that both diffusion and Shockley-Read-Hall (SRH) recombination processes contribute to the forward dark current.

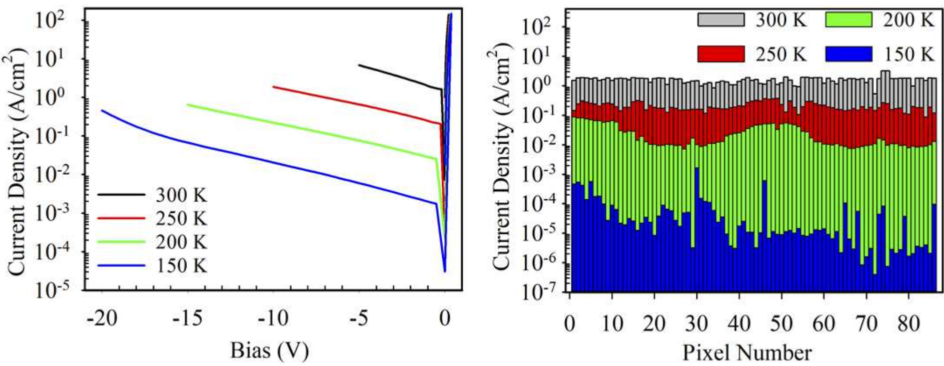

Fig. 2. Mean current-voltage characteristics of 87 devices measured at different temperatures (left) and dark current per pixel at a bias of −0.5 V (right).

The dark currents of each pixel at four temperatures for 87 pixels are shown in Fig. 2 (right). The mean and standard deviation of the dark current at −0.5 V, at these temperatures are compared

Optics EXPRESS

in Table 1. At 250 K and above, the standard deviation of the dark current is much less than the mean and the pixels appear highly uniform. However, as the temperature is reduced, the standard deviation reduces at a slower rate than the mean, and by 150 K the standard deviation has surpassed the mean. Dark current analysis in [21] showed that at temperatures below 200 K, surface leakage becomes significant in Be implanted planar APDs which underwent similar surface treatment and passivation to the ones presented here. Hence, this is likely to be the result of increased dominance of the surface leakage component from the top InAs surface as the bulk dark current becomes lower. This suggests the need to also improve the surface resistivity. The dark current density is still ~ 5 orders of magnitude higher than the 3 µm cut-off HgCdTe photodiodes in [22]. Due to the continued presence of surface leakage and SRH recombination processes, further optimisation of the fabrication process and growth is required before the dark current InAs APDs can rival that of HgCdTe APDs with a similar cut-off wavelength.

Table 1. Mean and standard deviation of dark current density at −0.5 V

Temperature (K)	Mean (A/cm^2)	Standard Deviation (A/cm^2)
300	1.61	0.397
250	0.208	66.7×10^{-3}
200	26.0×10^{-3}	22.1×10^{-3}
150	79.7×10^{-6}	213×10^{-6}

The responsivities at −0.1 V, before the onset of avalanche gain, across 50 randomly selected devices at 1520 nm and 2004 nm were measured at room temperature. Room temperature responsivities in InAs photodiodes at these wavelengths have been shown to be independent of temperature down to 77 K [23]. The data are presented in Fig. 3. A larger area 200 µm diameter reference mesa diode fabricated from the same wafer using identical implant conditions is also included for comparison. The good agreement with the results from the reference diodes, suggests that the uncertainties arising from laser spot are small. The spread in responsivity was found to be 0.49 ± 0.017 and 0.89 ± 0.024 A/W under 1520 and 2004 nm illumination respectively. For comparison, the mesa linear array in [20] exhibited 2 µm responsivity of 0.6 A/W. Since the fiber was manually positioned on to the optical window, it could introduce some uncertainties in this spread. The responsivity values correspond to mean external quantum efficiencies of 40.1% at 1520 nm and 55.1% at 2004 nm. These values are modest and could be due to the unoptimized thickness of the AR coating, since it is the same thickness as the SiN layer required for bondpad deposition.

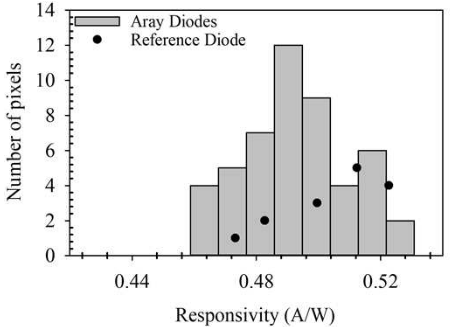

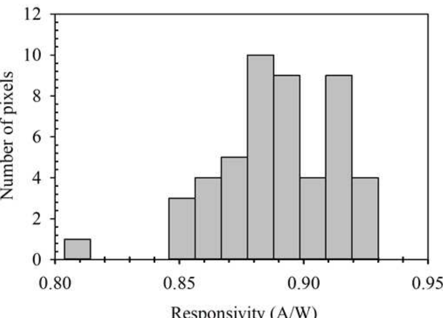

Fig. 3. Unmultiplied responsivity at 1520 (left) and 2004nm (right).

Optics EXPRESS

Avalanche gain data (mean and standard deviation) from 14 randomly selected planar APDs at 300 K and 200 K are shown in Fig. 4. The background doping in the intrinsic region was estimated to be $\sim 1.65 \times 10^{15}$ cm^{-3} from capacitance measurements. Hence, the devices would not be fully depleted before the onset of avalanche gain. The inset plot in Fig. 4. (left) shows the measured photocurrent between 0 and 1 V reverse bias. The initial sharp rise in photocurrent from 0 to 0.1 V is caused by widening depletion region, which improves collection efficiency of photo-generated carriers. The photocurrent remains constant between 0.1 and 0.5 V, indicating negligible change in the collection efficiency. This is not surprising considering the long minority carrier diffusion lengths in InAs (30 - 60 µm for electrons and 10 - 20 µm for holes [24]). Hence, the photocurrent values at reverse bias between 0.1 and 0.5 V are used as primary photocurrent for subsequent extraction of avalanche gains.

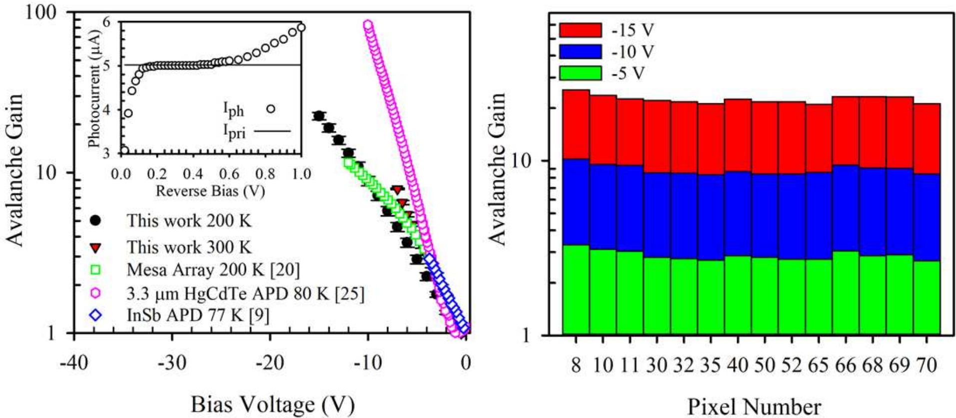

Fig. 4. Mean avalanche gain of the planar APD array measured at 300 K and 200 K, along with comparisons to a previously published mesa linear array, an InSb APD and a 3.3 µm cut-off HgCdTe APD (left) with an inset plot of the measured photocurrent (I_{ph}) with primary photocurrent (I_{pri}) and gain per pixel at different bias voltages (right).

At lower bias voltages the gain is slightly lower than the linear array of mesa APDs from [20]. However, at higher biases, gain from the planar APDs surpasses that of the mesa APDs. These small differences can be attributed to the wider intrinsic region used in this work compared with [20] (6 µm versus 4 µm) which requires a larger reverse bias to achieve full depletion. A consistent avalanche gain of around 22.5 ± 1.18 could be achieved at 200 K. At low bias (< 3 V) the gain is similar to the 3.3 µm cut-off HgCdTe APDs presented in [25].

4. Conclusion

Linear arrays of InAs planar APDs have been fabricated and characterized. Although the dark current is slightly higher than previously reported InAs mesa APDs, it is comparable to previously reported InAs planar APDs. The planar APDs exhibit uniform dark currents at 300 K and 250 K. At lower temperatures surface leakage currents appear to cause non-uniformity in the dark current. Responsivity and avalanche gain in these APDs appear to be highly uniform and a maximum gain of 22.5 ± 1.18 is achieved at 200 K. Further study is needed to improve the uniformity of the dark current at lower temperatures and assess crosstalk between planar InAs APD pixels. Our results demonstrate arrays of planar APDs with uniform gain and responsivities. Hence InAs APDs have the potential to be utilized as low-cost alternative SWIR and MWIR detectors.

Funding. Engineering and Physical Sciences Research Council (EP/S026428/1).

Optics EXPRESS

Acknowledgments. The authors would like to thank the National Epitaxy Facility for providing the wafers used in this work.

Disclosures. The authors declare no conflicts of interest.

Data availability. The data reported in this article are available in [26].

References

1. K. Ikuta, N. Yoshikane, N. Vasa, Y. Oki, M. Maeda, M. Uchiumi, Y. Tsumura, J. Nakagawa, and N. Kawada, "Differential Absorption Lidar at 1.67 µm for Remote Sensing of Methane Leakage," Jpn. J. Appl. Phys. **38**(1A), 110–114 (1999).
2. N. Menyuk and D. K. Killinger, "Atmospheric remote sensing of water vapor, HCl and CH_4 using a continuously tunable Co:MgF_2 laser," Appl. Opt. **26**(15), 3061–3065 (1987).
3. A. Minato, M. D. M. A. Joarder, S. Ozawa, M. Kadoya, and N. Sugimoto, "Development of a Lidar System for Measuring Methane Using a Gas Correlation Method," Jpn. J. Appl. Phys. **38**(10), 6130–6132 (1999).
4. T. F. Refaat, S. Ismail, G. J. Koch, M. Rubio, T. L. MacK, A. Notari, J. E. Collins, J. Lewis, R. De Young, Y. Choi, M. N. Abedin, and U. N. Singh, "Backscatter 2-µm Lidar Validation for Atmospheric CO_2 Differential Absorption Lidar Applications," IEEE Trans. Geosci. Remote Sensing **49**(1), 572–580 (2011).
5. C. Downs and T. Vandervelde, "Progress in Infrared Photodetectors Since 2000," Sensors **13**(4), 5054–5098 (2013).
6. M. S. Cabrera, C. W. McMurtry, W. J. Forrest, J. L. Pipher, M. L. Dorn, and D. Lee, "Characterization of a 15-µm cutoff HgCdTe detector array for astronomy," J. Astron. Telesc. Instrum. Syst. **6**(01), 1 (2019).
7. A. Singh, V. Srivastav, and R. Pal, "HgCdTe avalanche photodiodes: A review," Opt. Laser Technol. **43**(7), 1358–1370 (2011).
8. Y. Lin, S. Wang, and E. Steindal, "Minamata Convention on Mercury: Chinese progress and perspectives," Natl. Sci. Rev. **4**(5), 672–677 (2017).
9. J. Abautret, J. P. Perez, A. Evirgen, J. Rothman, A. Cordat, and P. Christol, "Characterization of midwave infrared InSb avalanche photodiode," J. Appl. Phys. **117**(24), 244502 (2015).
10. Y. Arslan, F. Oguz, and C. Besikci, "Extended wavelength SWIR InGaAs focal plane array: Characteristics and limitations," Infrared Phys. Technol. **70**, 134–137 (2015).
11. Z. Xie, Z. Deng, X. Zou, and B. Chen, "InP-based near infrared/extended-short wave infrared dual-band photodetector," IEEE Photonics Technol. Lett. **32**(16), 1003–1006 (2020).
12. A. R. J. Marshall, C. H. Tan, M. J. Steer, and J. P. R. David, "Extremely low excess noise in InAs electron avalanche photodiodes," IEEE Photonics Technol. Lett. **21**(13), 866–868 (2009).
13. J. Beck, C. Wan, M. Kinch, J. Robinson, P. Mitra, R. Scritchfield, F. Ma, and J. Campbell, "The HgCdTe electron avalanche photodiode," J. Electron. Mater. **35**(6), 1166–1173 (2006).
14. D. C. Herbert, P. A. Childs, R. A. Abram, G. C. Crow, and M. Walmsley, "Self-consistent 2-D Monte Carlo simulations of InSb APD," IEEE Trans. Electron Devices **52**(10), 2175–2181 (2005).
15. R. D. Baertsch, "Noise and multiplication measurements in InSb avalanche photodiodes," J. Appl. Phys. **38**(11), 4267–4274 (1967).
16. A. R. J. Marshall, C. H. Tan, J. P. R. David, J. S. Ng, and M. Hopkinson, "Fabrication of InAs photodiodes with reduced surface leakage current," in *Proc. SPIE, Opt. Mater. Def. Sys. Technol.* (IEEE, 2007), p. 67400H.
17. B. S. White, I. C. Sandall, J. P. R. David, and C. H. Tan, "InAs Diodes Fabricated Using Be Ion Implantation," IEEE Trans. Electron Devices **62**(9), 2928–2932 (2015).
18. L. W. Lim, C. H. Tan, J. S. Ng, J. D. Petticrew, and A. B. Krysa, "Improved Planar InAs Avalanche Photodiodes with Reduced Dark Current and Increased Responsivity," J. Lightwave Technol. **37**(10), 2375–2379 (2019).
19. P. J. McNally, "Ion implantation in InAs and InSb," Radiation Effects **6**(1), 149–153 (1970).
20. I. C. Sandall, S. Zhang, and C. H. Tan, "Linear array of InAs APDs operating at 2 µm," Opt. Express **21**(22), 25780 (2013).
21. B. S. White, I. C. Sandall, X. Zhou, A. Krysa, K. McEwan, J. P. R. David, and C. H. Tan, "High-Gain InAs Planar Avalanche Photodiodes," J. Lightwave Technol. **34**(11), 2639–2644 (2016).
22. O. Gravrand, J. Rothman, C. Cervera, N. Baier, C. Lobre, J. P. Zanatta, O. Boulade, V. Moreau, and B. Fieque, "HgCdTe Detectors for Space and Science Imaging: General Issues and Latest Achievements," J. Electron. Mater. **45**(9), 4532–4541 (2016).
23. P. J. Ker, A. R. J. Marshall, J. P. R. David, and C. H. Tan, "Low noise high responsivity InAs electron avalanche photodiodes for infrared sensing," Phys. Status Solidi C **9**(2), 310–313 (2012).
24. M. P. Mikhailova, in *Handbook Series on Semiconductor Parameters, Vol. 1: Si, Ge, C (Diamond), GaAs, GaP, GaSb, InAs, InP, InSb.* (World Scientific Publishing Co. Pte. Ltd., 1996), Chap. 7, pp. 147–167.
25. J. Rothman, K. Foubert, G. Lasfargues, C. Largeron, I. Zayer, Z. Sodnik, M. Mosberger, and J. Widmer, "High operating temperature SWIR HgCdTe APDs for remote sensing," Proc. SPIE **9254**, 92540P (2014).
26. T. Osman, L. W. Lim, J. S Ng, and C. H. Tan, "Data for Fabrication of infrared linear arrays of InAs planar avalanche photodiodes," The University of Sheffield, ORDA digital repository (2022) [retrieved 27 May 2022], https://doi.org/10.15131/shef.data.19509001.v1.